Polarization transitions in one-dimensional arrays of interacting rings

Bahman Roostaei,[1,2] Kieran J. Mullen,[3] and A. T. Rezakhani[4]
[1]*Department of Physics and Astronomy, Case Western Reserve University, Cleveland, Ohio 44106, USA*
[2]*Homer L. Dodge Department of Physics and Astronomy, University of Oklahoma, Norman, Oklahoma 73019, USA*
[3]*Department of Physics and Astronomy, University of Oklahoma, Norman, Oklahoma 73019, USA*
[4]*Center for Quantum Information Science and Technology, Department of Chemistry and Physics, University of Southern California, Los Angeles, California 90089, USA*
(Received 2 May 2006; revised manuscript received 16 July 2008; published 12 August 2008)

Periodic nanostructures can display the dynamics of arrays of atoms while enabling the tuning of interactions in ways not normally possible in nature. We examine one-dimensional (1D) arrays of a "synthetic atom," a one-dimensional ring with a nearest-neighbor Coulomb interaction. We consider the classical limit first, finding that arrays of singly charged rings possess antiferroelectric order at low temperatures when the charge is discrete, but that they do not order when the charge is treated as a continuous classical fluid. In the quantum limit Monte Carlo simulation suggests that the system undergoes a quantum phase transition as the interaction strength is increased. This is supported by mapping the system to the 1D transverse field Ising model. Finally, we examine the effect of magnetic fields. We find that a magnetic field can alter the electrostatic phase transition producing a ferroelectric ground state, solely through its effect of shifting the eigenenergies of the quantum problem.

DOI: 10.1103/PhysRevB.78.075411 PACS number(s): 73.21.−b, 73.22.−f, 73.43.Nq, 77.80.−e

I. INTRODUCTION

Fabrication of micro- and nanosized structures such as quantum dots, wires and rings has made it possible for physicists to examine new ideas in electronic devices. These small size devices act as artificial atoms with spectra and shell structures similar to those of real atoms.[1] However, it is possible to control the properties of these synthetic atoms in a way that is impossible with real ones. For example, a regular atomic orbital is three dimensional and one has limited control over the electronic wave function. In contrast, by controlling the shape of a quantum dot we can distort the wave function, controlling its polarizability and its interaction with adjacent dots. While the properties of periodic arrays of atoms are well understood in solid-state physics, we have a new playing field—periodic arrays of nanostructures—in which we have an unprecedented control of the "atomic states."

The focus of this paper is on periodic one-dimensional (1D) arrays of nanorings. We chose this system for two reasons. First, quantum rings display interesting phenomena (e.g., persistent currents[2–5]) which are not found in dots. The basic difference between the ring geometry and a quantum dot is the excluded middle which confines the electron in a ring to a narrow spatially periodic channel. This compact, periodic geometry can allow dynamics not found in other systems.[6] Second, it has become possible to create extremely small rings. These arrays of nanorings can be fabricated either by dry etching[7] or by using molecular beam epitaxy (MBE) techniques to foster self-assembled InGaAs/GaAs rings. The size of these nanorings is ~30 nm for outer radius and ~10 nm for inner radius for self-assembled InGaAs/GaAs rings.[8–10] These rings will often form in small clusters. Such techniques not only produce extremely small rings but also make it easy to make *periodic* arrays of small rings.

In this paper we consider an ideal array of 1D rings at zero temperature, each carrying a single charge. The rings are sufficiently close together that there is a Coulomb interaction between the electrons, but separated enough so that the tunneling between rings can be neglected,[11] as discussed in Sec. II. In Sec. III we consider the classical case and see how different assumptions allow for symmetric or symmetry breaking ground states. Section IV contains the main results of this work, where we show that there is a *quantum phase transition* in a 1D array of rings for $B=0$. We show this both through Monte Carlo simulation of $1+1D$ classical statistical representation of the problem as well as mapping it onto the 1D transverse field Ising (TFI) model. The polarization pattern is antiferroelectric. In Sec. V we examine how this transition is affected by magnetic fields. We conclude in Sec. VI by summarizing results and discussing possible applications.

II. MODEL

We consider a one-dimensional array of singly charged narrow quantum rings with radius R and center-to-center separation of D (Fig. 1). The width of each ring is much smaller than its inner radius so that we need only consider the one-dimensional movement of the electron around the ring. While the rings are isolated from each other so that

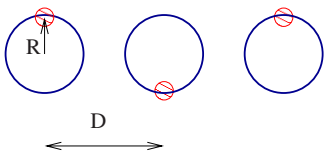

FIG. 1. (Color online) A schematic picture of the ground state of classical point electrons for 1D array of rings. The ring radius is R and the separation is D. The 1D ordering is antiferroelectric for the infinite size system and thus has a double degenerate ground state.

there is no charge transfer between rings, the rings still interact electrostatically with their nearest neighbors.[11] While in principle the Coulomb interaction is long range, we assume that there is sufficient screening that next-nearest-neighbor interactions can be neglected.

We also neglect tunneling between rings. This is reasonable since the physical realizations discussed above produce rings that are not in tunneling contact. Tunneling will be exponentially suppressed with D, so that for spatially distinct rings it will be minimal.

All the phenomena explained in this article will only appear in experiments if the electrons do not lose their quantum mechanical phase, i.e., the ring's perimeter has to be smaller than the electron's coherence length ($2\pi R < L_\phi$) and the temperature has to be lower than the dephasing temperature ($T < T_\phi$). In each ring the confinement energy of the electron scales as $E_q = \hbar^2/2m^*R^2$; this energy opposes localization of the wave function in the ring. The inter-ring Coulomb repulsion, which scales as $E_c = e^2/D$, tries to localize the wave function. Electrons are repelled from regions of the ring where it is too close to the charges on neighboring rings. The competition between these two physical scales creates a *quantum phase transition* in the array from a localized state to extended state as we will see below.

III. CLASSICAL RESULTS

Before solving a quantum mechanical problem, it is often helpful to look at the similar classical case which is usually easier to solve. Below we consider two classical models, one in which the classical charges are treated as ideal points, and the second in which they are treated as a continuous fluid.

A. Classical point charges

The classical model considers one charged point particle per ring with only nearest-neighbor Coulomb interaction. Unlike the quantum mechanical case, there is only one energy scale in the classical problem, the Coulomb energy $E_c = e^2/D$. The energy of a 1D array is given by $U_{1D} = \Sigma_{i=1}^{N} e^2/|\vec{r}_i(\theta_i) - \vec{r}_{i+1}(\theta_{i+1})|$, where θ_i is the location of the i-th electron as measured from the horizontal axis. In the dipole approximation we can write this as

$$U_{1D} - U_0 \approx \frac{\epsilon^2 e^2}{2D} \sum_i [3\cos 2\theta_i + \cos(\theta_i - \theta_{i+1}) - 3\cos(\theta_i + \theta_{i+1})] = \frac{\epsilon^2 e^2}{D} \sum_i \left\{ \vec{s}_i \cdot \vec{s}_{i+1} + \frac{3}{2}[\hat{D} \cdot (\vec{s}_i - \vec{s}_{i+1})]^2 \right\}, \quad (1)$$

where $\epsilon \equiv R/D$ and U_0 is a constant, $U_0 \equiv \frac{Ne^2}{D}(1 + \frac{\epsilon^2}{2})$. In the second expression we identify the position of each charge by a vector $\vec{s}_i$ in the two-dimensional (2D) plane pointing from the center of the i-th ring to the charge on that ring. The unit vector $\hat{D}$ lies on the horizontal axis.

The $\cos 2\theta$ [or $(\hat{D} \cdot \vec{s})^2$] term explicitly breaks the rotational symmetry, driving the system from XY to Ising-type behavior. The Heisenberg term in the last line of Eq. (1) drives the system ferroelectric (FE) at zero temperature, while the second and larger term favors states where neighbors point in the opposite direction. Thus, the system at zero temperature orders in an antiferroelectric (AFE) pattern (Fig. 1) in one dimension. Our numerical Monte Carlo simulations of the exact Coulomb interaction also verify the existence of such a minimum energy configuration in the classical finite-size arrays.

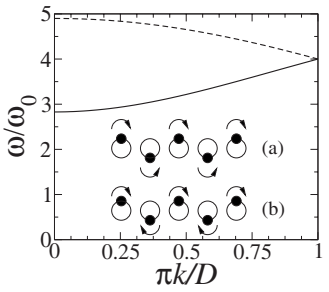

FIG. 2. Normal modes of the 1D ring array with gaps of [solid line, inset (a)] $2\sqrt{2}\omega_0$ and [dashed line, inset (b)] $2\sqrt{6}\omega_0$, where $\omega_0 = \sqrt{e^2/m^*D^3}$.

We can examine the stability of the AFE state by finding the higher energy modes of the system. We expand the energy function [Eq. (1)] to quadratic order in displacement angle around the AFE configuration using $\theta_i = (-1)^i \frac{\pi}{2} + \alpha_i$. The AFE configuration has a basis with two sites so we find two independent normal modes with frequencies:

$$\omega_{\pm}^{(1D)}(k) = 2\omega_0 \sqrt{4 \pm 2\cos\frac{kD}{2}}, \quad (2)$$

where $\omega_0 \equiv \sqrt{e^2/m^*D^3}$. Both the modes are gapped since the Ising-type term provides the harmonic restoring force at each site. The modes are shown in Fig. 2. Normal modes are found to be independent of the ring radius.

B. Classical charge fluid

Another interesting classical limit of our ring problem is when there is a classical *self-interacting* fluid of charge on each ring while the nearest-neighbor fluids are still interacting with each other. To find the minimum energy distribution of charge density on each ring we define an angular dependent charge density $\rho_i(\theta_i)$ on each ring, where $\int \rho_i(\theta_i) d\theta_i = 1$. We are looking for the minimal solution to the variational quantity:

$$I = \frac{1}{2} \int d\theta \int d\theta' \sum_{\langle ij \rangle} \frac{\rho_i(\theta)\rho_j(\theta')}{|\vec{r}_i - \vec{r}_j|} + \lambda \sum_i \int d\theta \rho_i(\theta). \quad (3)$$

For a 1D ring this expression is divergent due to self-energy. We can regularize this in several ways. One method is to introduce a short distance cutoff ζ to the Coulomb interaction, discretize the integral equation, and then solve the problem numerically. An approximate analytic solution can then be obtained by Fourier expanding the distribution, keeping only the first three modes.

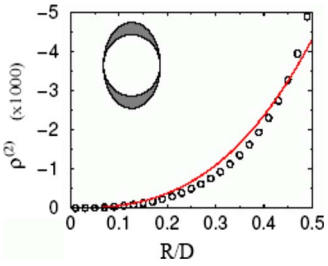

FIG. 3. (Color online) A plot of the second Fourier amplitude of the classical charge distribution on a ring in a 1D horizontal array. The circles are numerical results; the solid line is a scaled plot of Eq. (4). Scaling is required since the analytic result neglects all higher Fourier modes. Inset: a sketch of the charge distribution that corresponds to this Fourier mode. Note that the symmetry of the array is not broken by the charge distribution.

For 1D array with periodic boundary condition we find that the amplitude of the nontrivial Fourier mode as a function of ζ and $\epsilon \equiv R/D$ for ρ is given by

$$\hat{\rho}^{(2)} \approx \frac{-3\pi\epsilon^3(2-5\zeta^2)}{4[-2+4\log(\epsilon/\zeta)]}. \tag{4}$$

We compare this analytic result with the numerical diagonalization of Eq. (3) in Fig. 3. As we can see in Fig. 3 the minimum energy configuration of the 1D array of charge fluid does not break the up-down symmetry of the system.

IV. QUANTUM RESULTS FOR $B=0$

At first glance the quantum mechanical wave function of a charged particle resembles the classical charge fluid. Although the wave function does not have a self-interaction, the quantum particle has a kinetic energy which opposes localization, making the analogy to charge fluid even stronger. Unlike the classical case, the quantum problem has two competing energy scales: the quantum kinetic energy, E_q, preventing localization and the Coulomb interaction energy, E_c, trying to force the charges away from each other. At $E_q \ll E_c$ we expect charge localization on each ring and at $E_q \gg E_c$ we expect no localization of charge. However, it is not *a priori* obvious whether the charge localization (system polarization) breaks symmetry or not, whether this localization is a smooth function of the external parameters, and if it is a phase transition, what is the exact nature of this transition.

A. Variational calculation

As a first step we can use a simple variational wave function to find the polarization behavior of the system in ground state. The dimensionless Hamiltonian of an array of one-dimensional rings with radius R is given by

$$\hat{H} = -\sum_i \frac{\partial^2}{\partial\theta_i^2} + \delta\sum_{\langle ij\rangle} \frac{1}{|\vec{r}_i'(\theta_i) - \vec{r}_j'(\theta_j)|}, \tag{5}$$

where $\vec{r}' = \vec{r}/R$ and $\delta = E_c/E_q$ is the interaction strength and the energy is measured in units of $E_q = \hbar^2/2mR^2$.

To find the ground-state energy of the 1D array we employ a simple ansatz for the wave function of each sublattice: $\psi_A(\theta) = \frac{\sqrt{1-y^2}}{\sqrt{2\pi}} + \frac{y}{\sqrt{2\pi}}\cos(\theta-\phi)$ and $\psi_B(\theta) = \frac{\sqrt{1-y^2}}{\sqrt{2\pi}} - \frac{y}{\sqrt{2\pi}}\cos(\theta-\phi)$ alternately. The ground-state values of y and ϕ are obtained by minimizing the energy [Eq. (5)]. Using dipole approximation for Coulomb interaction we find

$$y(\delta,\epsilon) = \begin{cases} \frac{1}{4}\sqrt{11 - \frac{4}{\delta\epsilon^2}} & \text{for } \delta \geq \delta_c(\epsilon) \\ 0 & \delta < \delta_c(\epsilon) \end{cases} \tag{6}$$

and $\phi = \pi/2$, where the critical value of the interaction is given by $\delta_c(\epsilon) = \frac{4}{11}\epsilon^{-2}$. To find out the degree of polarization we define the *staggered polarization* vector as

$$\vec{P}_s = \sum_i (-1)^i \int d\theta |\psi_i(\theta)|^2 \vec{r}_i(\theta). \tag{7}$$

Using variational results the staggered polarization of the system is as follows:

$$\vec{P}_s(\delta,\epsilon) = \begin{cases} \frac{1}{8}\left(\frac{4+5\delta\epsilon^2}{2\delta\epsilon^2}\right)^{1/2}\left(11 - \frac{4}{\delta\epsilon^2}\right)^{1/2}\hat{D}_\perp & \delta \geq \delta_c \\ 0 & \delta \leq \delta_c \end{cases}, \tag{8}$$

where $\hat{D}_\perp$ is the unit vector perpendicular to the common axis of the rings (Fig. 1) and δ_c is defined in Eq. (6).

As we can see, variational calculation suggests that the ground state of the 1D array of rings antiferroelecrically polarizes in perpendicular direction at high interaction strengths while at lower values the wave functions are not localized, hence the system has no polarization. The validity of this result will be confirmed in next sections using more exact and reliable methods of calculation.

B. Hartree approximation

The rings considered here are well separated with exactly one electron on each ring. Under this condition and because of strong Coulomb repulsion the effect of inter-ring transfer of electrons and overlap of wave functions is small. We can therefore neglect the inter-ring transfer from our calculations. Since without overlap the electrons do not have any exchange interaction, the Hartree approximation is exact for this problem.[12]

We can decompose the wave function in each ring into a limited number of Fourier modes, $\psi_i(\theta) = \Sigma_{n=-n_0}^{n_0} c_n e^{in\theta}$, and then solve the system numerically in the Hartree approximation. We impose the periodic boundary conditions on the array and by an iterative self-consistent method we find the ground-state wave function of the rings. In Fig. 4 we can see the numerical results of the polarization and energy change of the 1D array of rings for different number of Fourier modes using exact Coulomb interaction and also its agreement with the variational calculation when we restrict the number of Fourier modes to $n \in \{-1,0,1\}$. The results are changed little when we increase the number of Fourier modes mostly in the high coupling regime.

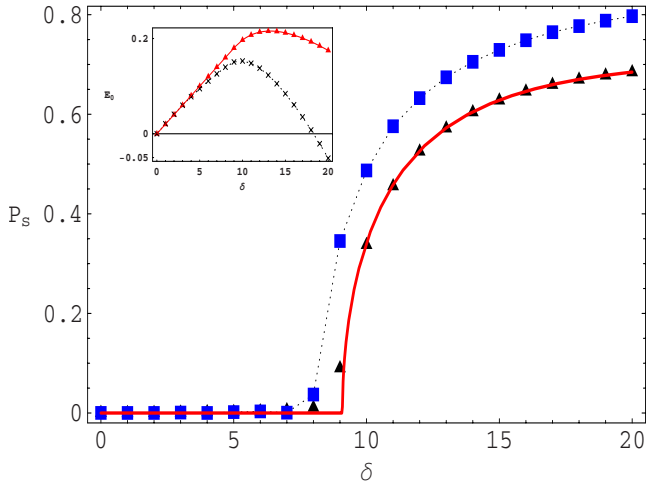

FIG. 4. (Color online) A comparison of numerical and analytical calculations of the staggered polarization and energy as a function of δ in a 1D quantum ring array obtained in the Hartree approximation. The numerical results for the case include Fourier modes $|m| \leq 1$ (triangles) and $|m| \leq 6$ (boxes). The solid line is the analytic result assuming $|m| \leq 1$. The quantity δ is a measure of the competition between the Coulomb interaction and the quantum kinetic energy.

All the above results suggest that there is transition from unpolarized to polarized state at zero temperature by changing the coupling. By looking at the behavior of polarization when the number of Fourier modes increases we realize that this transition tends to be sharper and sharper for higher number of Fourier modes suggesting a true phase transition in the system. If true, this transition would be a sudden change in ground state of the quantum system at zero temperature known as *quantum phase transition*.[13] We demonstrate that this is the case and determine the universality class of the transition in Sec. IV C using the Monte Carlo simulation.

C. Monte Carlo simulation

It is well known that we can write the quantum partition function of a quantum system, $Z=\mathrm{Tr}\, e^{-\beta \hat{H}}$, as the sum over all paths taken by the system in imaginary time defined by the scale $\hbar\beta$. If the quantum system is D dimensional then the partition function will look like the path integral of a $D+1$–dimensional classical system in which the extra dimension is the time direction $0 < \tau < \beta\hbar$. At zero temperature $\beta \to \infty$ the classical system is truly $D+1$ dimensional. One can derive an effective Hamiltonian for such a classical system from the quantum Hamiltonian using a complete set of basis states. In this classical system the parameters of the quantum system (in our case δ) is a control knob like temperature. We can use Monte Carlo simulation of such a classical system and find out the universal behavior of the quantum system.

To develop a $1+1$–dimensional classical theory for our 1D ring array we first stagger the order parameter, $\theta_i \to (-1)^i \theta_i$ so that we can analyze the Monte Carlo results easily. We also use dipole approximation for the Coulomb interaction. Consequently, we can write the Hamiltonian of the system as

$$\hat{\mathcal{H}} = \frac{E_c}{2} \sum_{j=1}^{N} \left(-i \frac{\partial}{\partial \theta_j} \right)^2 - E_J \sum_{j=1}^{N} \hat{V}, \tag{9}$$

in which $E_c = \hbar^2/mR^2$ and $E_J = e^2\epsilon^2/2D$. The standard derivation[14] using the Villain approximation[15,16] tells us that the $1+1D$ classical partition function equivalent to the 1D interacting quantum ring array at zero temperature is

$$Z \propto \int \mathcal{D}\theta(\tau) \prod_{a=1}^{\mathcal{N}} \exp\left\{ \frac{\hbar}{E_c \delta\tau} \sum_{k=1}^{N} \cos[\theta_k(\tau_{a+1}) - \theta_k(\tau_a)] + \frac{\delta\tau E_J}{\hbar} \sum_{k=1}^{N} V_k(\tau_a) \right\}, \tag{10}$$

where $\mathcal{D}(\theta) \equiv \Pi_{a=1}^{\mathcal{N}} D\theta(\tau_a)$ and

$$V_k(\tau_a) = 3\cos[\theta_k(\tau_a) - \theta_{k+1}(\tau_a)] + \cos[\theta_k(\tau_a) + \theta_{k+1}(\tau_a)] - 3\cos[\theta_k(\tau_a) - \theta_{k+1}(\tau_a)]\cos[\theta_k(\tau_a) + \theta_{k+1}(\tau_a)]. \tag{11}$$

The parameter τ has the dimension of time and $\mathcal{N}\delta\tau = \beta\hbar$. It can be shown that the field $\theta(x,\tau)$ obeys the periodic boundary condition, $\theta(\tau+\beta\hbar) = \theta(\tau)$ (Ref. 17). We will also assume periodic boundary condition in the space direction all over the simulation.

By defining the spin vector $\vec{S}_i = (\cos\theta_i, \sin\theta_i)$ we can interpret Eq. (10) as a two-dimensional classical spin model. Our early calculations suggested that the system of 1D rings has a transition from the unpolarized to the AFE state. In this classical analog because we have already staggered the order parameter we expect to see a transition from unpolarized to ferromagnetically polarized state (FE). Close to this transition the spatial variation of the order parameter $\vec{S}$ is smooth so we can approximate Eq. (11) as follows:

$$V_k(\tau_a) \approx 3\cos[\theta_k(\tau_a) - \theta_{k+1}(\tau_a)] - 2\cos 2\theta_k(\tau_a). \tag{12}$$

Using the above potential finally, the classical partition function looks like

$$Z \propto \int \mathcal{D}\theta(\tau) \exp\left\{ K \sum_{\langle ij \rangle} \cos(\theta_i - \theta_j) - \frac{2K}{3} \sum_i \cos 2\theta_i \right\}, \tag{13}$$

where i and j run over an infinite 2D square lattice and we have determined $\delta\tau$ to identify the two couplings in Eq. (10) as $K = \sqrt{\frac{3E_J}{E_c}}$. Equation (13) is a 2D XY model with a symmetry breaking field which is 2/3 the XY coupling. Our Monte Carlo analysis shows that this model has a continuous phase transition. The order parameter of this system is the total magnetization density equivalent to the total staggered polarization of the 1D ring array:

$$\vec{m} \equiv \langle \vec{S} \rangle \leftrightarrow \vec{P}_s, \tag{14}$$

where the average on the left-hand side is the thermodynamic average over the infinite size lattice.

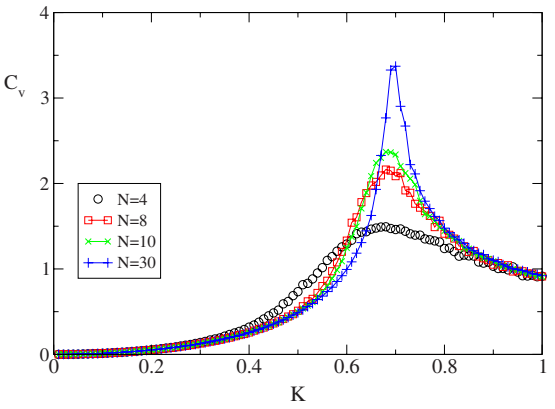

FIG. 5. (Color online) Monte Carlo results of the $\tilde{C}_v = \Delta E^2/N^2$ for different system sizes. The system is a $1+1D$ classical equivalent of a 1D quantum ring array at zero temperature.

The fluctuations in this system is controlled by K which is the analog of $1/T$ in real classical systems. We can measure the analog of specific heat of the system using

$$\tilde{C}_v = \frac{1}{N^2}(\langle E^2\rangle - \langle E\rangle^2) \tag{15}$$

in which $\langle . \rangle$ is the average over an ensemble and E is the total energy of the $N \times N$ system. This quantity diverges at the critical point of the infinite system undergoing a continuous phase transition. Figure 5 shows the change in the specific heat of our $1+1D$ system in terms of the parameter K for different lattice sizes. As we can see, at K_c the peak gets sharper and sharper with increasing lattice size L. An extrapolation of the point of the maximum of C_v, $K_c(L)$ to $L^{-1}=0$ determines the approximate critical point of the infinite lattice (Fig. 6). Also, an extrapolation of $m(L,K)$ for different values of K in Fig. 7 shows that a real continuous phase transition happens in the infinite size system.

The effective classical system derived here does not fully explain all the physical aspects of the 1D quantum system mainly because of the approximations used to derive the path integral. However, we believe that, close to the critical region, these approximations do not play any role in the general behavior of the system and the universality class remains unchanged. Hence, using the finite-size scaling method we can determine the critical exponents of the classical system

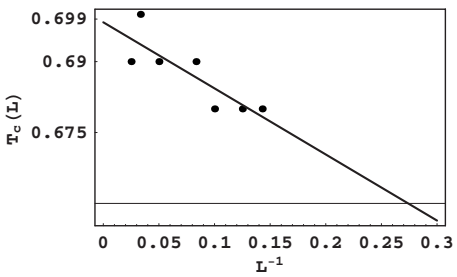

FIG. 6. Plot of critical coupling $K_c(L)$ at different system sizes taken from the C_v plots. The solid line is a linear fit to the data indicating $K_c(\infty) \approx 0.699$.

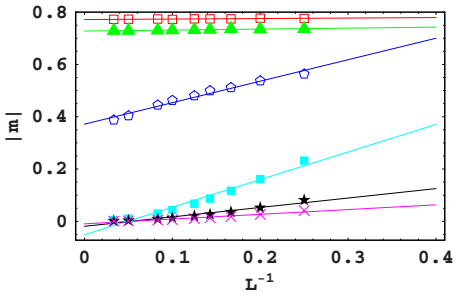

FIG. 7. (Color online) Extrapolation of the total magnetization density of the $1+1D$ classical system to infinite size at couplings $K/K_c(\infty)=1.45$ (empty boxes), 1.32 (triangles), 1.03 (polygons), 0.74 (filled boxes), 0.45 (stars), and 0.16 (crosses). The solid lines are linear fit to each set of data.

and determine the universality class of the actual quantum system.

1. Finite-size scaling of the 1+1D system

One of the best parameters for examining the phase transition and finding the universal exponents with finite-size scaling is the dimensionless Binder ratio,

$$g_L = \frac{\langle m^4\rangle}{\langle m^2\rangle^2}, \tag{16}$$

defined for a system with size L. In the disordered phase $K < K_c$ the correlation length ξ is finite so for $L \gg \xi$ the distribution of m is Gaussian around $m=0$ with the width $\sim N^{-1/2} \sim L^{-d/2}$ so $g \to 0$. On the other hand, for $K > K_c$ where $\langle m\rangle$ is finite, g_L approaches a constant as $L \to \infty$. The variation of g_L with K becomes sharper and sharper as L increases, however, all the g's cross at the transition point K_c. The variation is given by the following finite-size scaling function:

$$g_L(K) = \tilde{g}[L^{1/\nu}(K - K_c)], \tag{17}$$

where $\tilde{g}$ is a scaling function which depends on L and K only in that particular form. By using the finite-size data we can try to find a data collapse and by calculating the standard deviation find the best exponent ν fitting to the collapsed function. Figure 8 shows the Binder ratio for different lattice

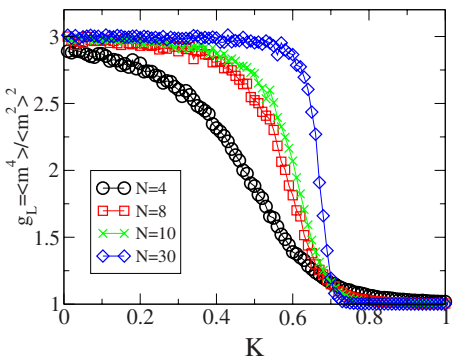

FIG. 8. (Color online) Plots of Binder ratio for different system sizes. The behavior is sharper at larger sizes.

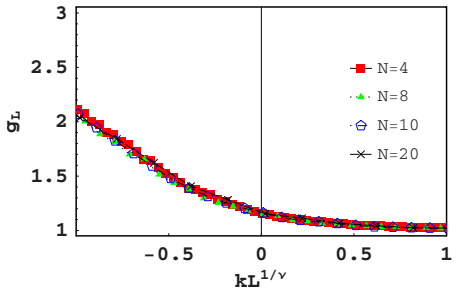

FIG. 9. (Color online) Collapse of Binder plots at the critical region. The best collapse is obtained for $\nu=1.01\pm.01$.

sizes. Figure 9 shows the collapsed data and Fig. 10 shows the best exponent is $\nu=0.99\pm0.01$. The error is estimated from the mesh of the numerical calculation.

The scaling for the order parameter $|m|$ is

$$m = L^{-\beta/\nu}X^0[L^{1/\nu}(K-K_c)], \tag{18}$$

where X^0 is a function of $x=L^{1/\nu}(K-K_c)$ only and β is one of the universal scaling exponents of the system. To determine the universal exponent β we plot $L^{\beta/\nu}$ vs x for different sizes (Fig. 11). Figures 12 and 13 show the collapse of different data sets and the standard deviation for different exponents, respectively, which shows the best estimation is $\beta=0.125\pm.005$, or 1/8.

2. Universality class

The universal exponents extracted from the finite-size data indicate that our $1+1D$ classical XY model in the symmetry breaking field is in the universality class of 2D classical Ising model, hence the nature of quantum phase transition of our 1D quantum ring array is Ising-type. The Coulomb repulsion forces the electrons to alternate staying on the top and bottom of the rings. However, the quantum kinetic energy tries to avoid localization. This kinetic energy causes the electrons to tunnel from top to bottom of the ring hence destroying the antiferroelectric order. This ordering behavior shows up in the probability distribution on each ring. Figure 14 shows the energy of each electron with the wave function $\psi_d(\theta)=x+y\cos(2\theta)$ compared to when the wave function is a constant all around the ring. The wave function ψ_d has two maxima on the top and bottom of the ring which means the electron is fluctuating up and down. As

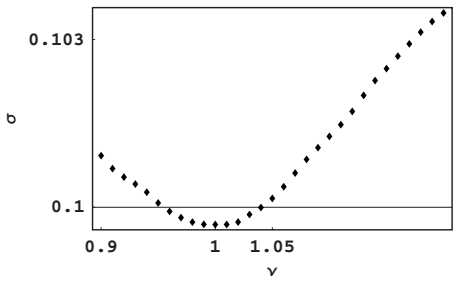

FIG. 10. Standard deviation of the set of scaled plots of Binder ratio for different exponents. The case for $\nu=1$ is the best choice which is plotted in Fig. 9.

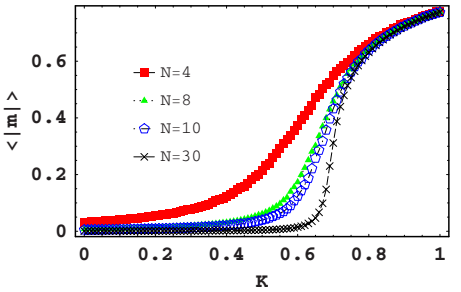

FIG. 11. (Color online) Monte Carlo results of average magnetization of the $1+1D$ classical system for different system sizes. The change in magnetization tends to be sharper as the system size grows.

we can see by increasing the coupling the lower energy state selected by the exact Hartree calculations (dots) gradually matches ψ_d instead of the constant wave function. This behavior persists in a range of couplings close but smaller than the critical coupling, i.e., in disordered region $\delta<\delta_c$. Needless to say, after transition point the ground-state wave function is no longer ψ_d and the system starts to excite more angular momentum eigenstates (Fourier modes).

All the above discussion suggests that the nature of the antiferroelectric transition is not just the simple 2D Ising but is similar to 1D TFI which has a quantum phase transition at zero temperature in the same universality class as 2D Ising. We can develop an effective 1D TFI Hamiltonian for our ring array in the dipole approximation. In this approximation we can write down the Hamiltonian (9) as follows:

$$\hat{H} = \hat{H}_0 + \hat{V},$$

$$\hat{H}_0 = \sum_i \left[\left(-i\frac{\partial}{\partial\theta_i}\right)^2 + 3\delta\epsilon^2\cos 2\theta_i\right],$$

$$\hat{V} = -\delta\epsilon^2\sum_i [3\cos(\theta_i+\theta_{i+1}) + \cos(\theta_i-\theta_{i+1})]. \tag{19}$$

The $\cos 2\theta$ term in Hamiltonian $\hat{H}_0$ has two minima at the top and bottom of the ring. Figure 15 shows the potential and the two lowest energy states of it with energies $E_0<E_1$. The rate of tunneling from top to bottom or vice versa is determined by $\Delta\equiv E_1-E_0$. The potential $\hat{V}$ tries to align the electrons hence it acts like the Ising interaction. A more rigorous

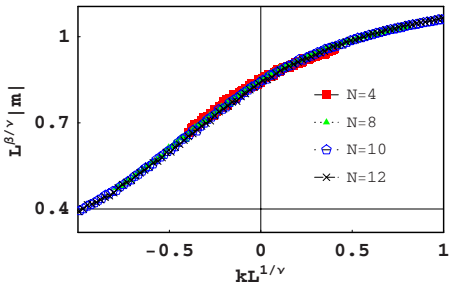

FIG. 12. (Color online) Collapse of scaled magnetization data sets for $\nu=1$ and $\beta=1/8$ in the critical region.

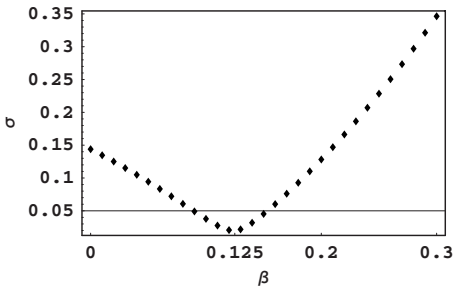

FIG. 13. Standard deviation of the set of scaled plots of magnetization for fixed $\nu=1$ and different exponent β. The case for $\beta=1/8$ is the best choice which is plotted in Fig. 12.

derivation using Holstein-Primakov bosons[18] shows that the projection of the Hamiltonian $\mathcal{H}$ into the subspace of the ground and first excited states of $\hat{H}_0$ can be written as (see Appendix)

$$\hat{H} \approx \Delta \sum_{i=1}^{N} \sigma_i^x - J \sum_{i=1}^{N} \sigma_i^z \sigma_{i+1}^z, \tag{20}$$

in which σ's are Pauli spin matrices and $J=8\delta\epsilon^2$. Numerical diagonalization of $\hat{H}_0$ tells us that $\Delta \approx 1-0.1\delta\epsilon^2$ for small ϵ.

Close to transition the Coulomb repulsion is not strong enough to excite the electrons to higher states, consequently the TFI model in Eq. (20) is valid and indicated the nature of transition of the 1D ring array.

V. QUANTUM RINGS TRANSITIONS FOR $B \neq 0$

Y. Aharonov and D. Bohm (AB) have predicted that the wave function of an electron moving in a vector potential $\vec{A}(x)$ along the path C acquires a phase shift:

$$\Delta\Lambda = \frac{e}{\hbar c} \int_C \vec{A} \cdot \vec{dr}. \tag{21}$$

AB predicted that this phase shift can be observable. When an electron is confined on a closed path like the case of

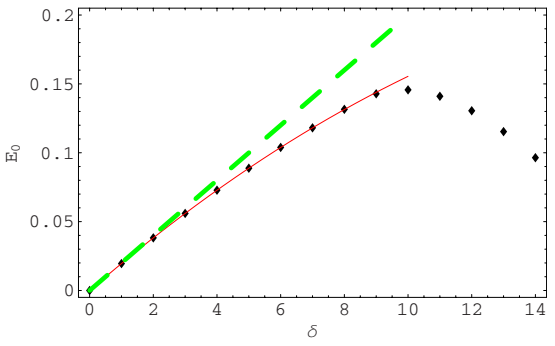

FIG. 14. (Color online) Plot of the energy of the interacting quantum ring array when all the wave functions are constant around the ring (dashed) or all are in the form of $\psi_d=a+b\cos 2\theta$ (solid). The points are the actual results coming out of the numerical Hartree calculation indicating that ψ_d is the selected behavior for $\delta < \delta_c \approx 8$.

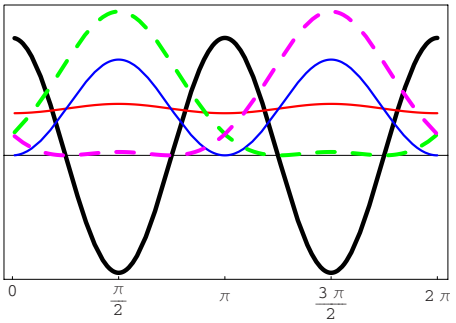

FIG. 15. (Color online) Plot of the $\cos 2\theta$ potential around a ring (the thick solid line), the ground and first excited state of this potential (thin solid lines) coming out of a simple numerical Schrodinger equation solver and the up and down states (dashed lines) constructed from the two eigenstates (see Appendix). The scale of the potential is exaggerated for easier comparison.

charged ring threaded by magnetic flux ϕ, the phase shift after one 2π rotation would be

$$\Delta\Lambda = \frac{e}{\hbar c} \oint \vec{A} \cdot \vec{dr} = \phi/\phi_0, \tag{22}$$

where $\phi_0=hc/e \simeq 4.135\times 10^{-7}$ G.cm^2 is the quantum of flux. The phase shift above has been observed in numerous experiments and different devices including the experiments of persistent current and excitons in quantum rings.[19] In this section we show how magnetic field changes the behavior of polarization.

The Hamiltonian of an electron in a 1D ring threaded by a constant uniform magnetic field $B\hat{z}$ (the ring is in the x-y plane) is

$$\hat{H} = \frac{\hbar^2}{2mR^2}\left(i\frac{\partial}{\partial\theta} + \frac{\phi}{\phi_0}\right) \tag{23}$$

in which the choice of gauge: $\vec{A}=\frac{B}{2}(-y,x,0)$, the momentum is in polar coordinates: $\hat{p}=-i\frac{\hbar}{R}\frac{\partial}{\partial\theta}$ and the eigenfunctions are periodic: $\psi(\theta+2\pi)=\psi(\theta)$. The eigenenergies of Eq. (23) will be

$$E_n = \frac{\hbar^2}{2mR^2}(n-\phi/\phi_0)^2 \tag{24}$$

in which n is an integer. By changing the gauge $\vec{A} \to \vec{A} - \nabla\Lambda$ wave functions undergo a phase change $\psi \to e^{ie/\hbar c\Lambda}\psi$. For example, we can use the gauge transformation with the choice of $\Lambda=(BR^2/2)\theta$ to remove the vector potential from Eq. (23) but at the same time we have to shift the phase of the wave functions to $e^{-i\phi/\phi_0\theta}\psi$. As a result the eigenfunctions change:

$$\psi_n(\theta) = \frac{1}{\sqrt{2\pi}} e^{i(n-\phi/\phi_0)\theta}. \tag{25}$$

This eigenfunction however, has a different boundary condition than the previous one:

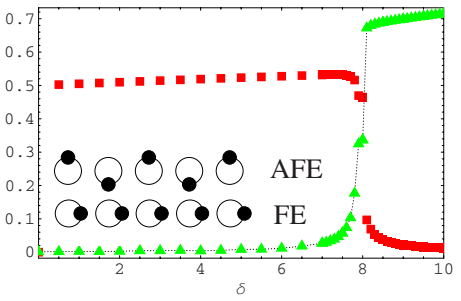

FIG. 16. (Color online) Results of numerical Hartree calculations of the polarization of a 1D quantum ring array threaded by half-flux quantum $\phi/\phi_0=1/2$. For $\delta<\delta_c$ the system displays a longitudinal FE polarization (squares), while for $\delta>\delta_c$ an antiferroelectric AFE polarization (triangles) is observed.

$$\psi(\theta+2\pi)=e^{2\pi i\phi/\phi_0}\psi(\theta) \tag{26}$$

but as one physically expects the eigenenergies are not changed. The ground-state energy of the interacting quantum ring array in the magnetic flux ϕ can be written as

$$E_0(\delta,\phi)=\sum_{n=-n_0}^{n_0}|c_n|^2(n-\phi/\phi_0)^2 + \delta\sum_{\langle ij\rangle}\int d\theta d\theta' \frac{|\Psi_0(\theta)|^2|\Psi_0(\theta')|^2}{|\vec{r}_i'(\theta)-\vec{r}_j'(\theta')|}, \tag{27}$$

where $\Psi_0(\theta)=e^{i\phi/\phi_0\theta}\Sigma_{n=-n_0}^{n_0}c_n e^{in\theta}$ is the ground-state wave function expanded in the free Hamiltonian basis states. As we can see in Eq. (27), the only part that is affected by the AB phase is the kinetic energy and the potential energy is not sensitive to the phase. The energy calculated in Eq. (27) is periodic in ϕ_0 since when $\phi=\phi_0=1$ we can rearrange the infinite sum and show that the value of the kinetic energy is equal to its value at $\phi=0$. This is due to the well-known fact that the physics of quantum rings does not change at integer flux quanta. For infinite n_0 this argument is true at any range of magnetic flux; in our numerical calculations where we have used a finite number of Fourier modes E_0 is periodic only in a finite range approximately given by $0<\phi<n_0\phi_0$. In Fig. 17 we can see the periodic behavior of the ground-state energy of the ring array as magnetic flux changes.

The results of our numerical Hartree calculations indicate that in a 1D ring array in which each ring is threaded by a magnetic flux ϕ the polarization pattern changes from unpolarized to ferroelectric at half-integer flux quantum. Figure 16 shows the behavior of P_x, the component of the total polarization vector $\vec{P}=\Sigma_i\int_0^{2\pi}d\theta|\psi_i(\theta)|^2\vec{r}_i(\theta)$ in the direction of the ring's common axis at half-flux quantum. This plot shows that at $\delta<\delta_c$ the wave function has an unbalanced distribution around each ring. However, the total polarization vanishes at higher values of interaction where the wave function distribution becomes antiferroelectrically polarized in the array. The finite polarization at small interaction strengths has a ferroelectric pattern which is degenerate left or right. From this result we can see that the physics of quantum ring arrays changes at half-integer flux quantum. The total staggered polarization in the $\hat{y}$ direction perpendicular to the common axis of the rings starts to build up at $\delta>\delta_c$ as in the case of no magnetic field. We can explain this phenomenon of *finite transverse polarization due to magnetic field* in different approaches.

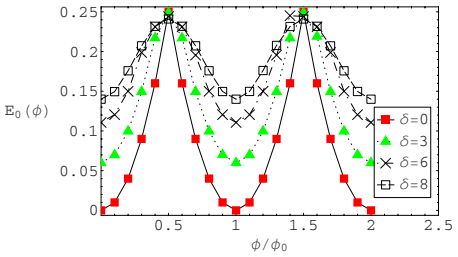

FIG. 17. (Color online) Plots of ground-state energy of the interacting quantum ring array in the external magnetic flux threading each ring for different couplings δ. The physics is periodic because of Aharonov-Bohm induced phase that is proportional to the flux.

We can use a simple perturbative discussion to understand this behavior qualitatively. Equation (19) which is the dipole approximation of the total Hamiltonian will modify in presence of a magnetic flux as follows:

$$\hat{H}=\hat{H}_0+\hat{V},$$

$$\hat{H}_0=\sum_i\left[\left(-i\frac{\partial}{\partial\theta_i}-\frac{\phi}{\phi_0}\right)^2+3\delta\epsilon^2\cos 2\theta_i\right],$$

$$\hat{V}=-\delta\epsilon^2\sum_i[3\cos(\theta_i+\theta_{i+1})+\cos(\theta_i-\theta_{i+1})]. \tag{28}$$

In the above equation the kinetic energy Hamiltonian has a degenerate ground state. For example at half filling, $\phi/\phi_0=\frac{1}{2}$, $n=0$ and $n=1$ levels are degenerate unlike the case of zero magnetic field in which the ground state is unique and at $n=0$. By adding the symmetry breaking term $\cos 2\theta$ in the case of zero flux the electron gains enough energy to excite to the next higher level. This excitation causes the electron to destroy any localization in the range where $\hat{V}$ is not strong enough yet. However, when there is a finite magnetic field the $\cos 2\theta$ cannot lift the degeneracy between $n=0$ and $n=1$ when δ is small. In this case the ground state of $\hat{H}_0$ remains degenerate (Fig. 17). As long as δ is small the perturbative two-body potential in Eq. (28) cannot excite the electron to higher levels and the kinetic energy of the electron freezes. When this happens the electrons behave classically and choose a wave function that minimizes the potential $\hat{V}$. In Fig. 18 we can see a three-dimensional (3D) plot of the two-body potential V in which it has two stable minima at (π,π) and (0,0) indicating the preferred state of the quantum ring array at low δ being the ferroelectric right or left state.

It is surprising that the system orders ferroelectrically along the chains. This occurs because the charge distribution is quite broad. Using only the two lowest Fourier modes the charge distribution can be written in general as $\rho(\theta)=[1+\cos(\theta-\theta_0)]/2\pi$, which nearly wraps around the ring. If we change this to a (unphysical) flat charge distribution with an

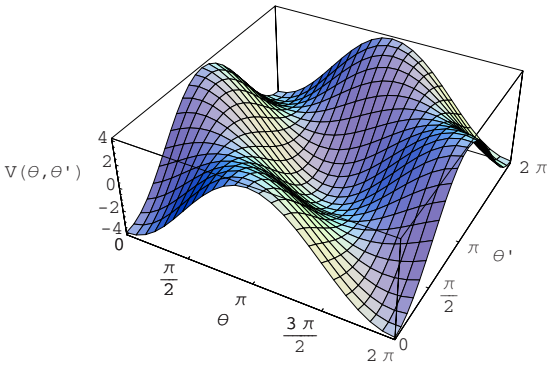

FIG. 18. (Color online) Plot of the two-body potential function in Eq. (28). The interacting rings in magnetic field select the minimum of this potential for their ground-state wave function at low couplings. The potential is in units of $\delta\epsilon^2$.

artificially varying width, the FE state has a lower energy than the AFE state when the width $\Delta\theta \sim .45\pi$, while for a triangular distribution the FE distribution is favored when $\Delta\theta \sim 0.6\pi$. While the exact transition depends of course upon ϵ, these calculations help explain why the FE phase wins out at half filling.

VI. CONCLUSIONS

In this paper we have shown that there is a phase transition in a periodic array of electrons each confined to a 1D ring. The parameter δ determines if the array will spontaneously polarize; in 1D the transition is at $\delta \approx 10$. It is easy to achieve small values of δ simply by choosing the ring separation to be large. Thus, the "quantum" limit where the kinetic energy dominates is simple to obtain. To obtain the antiferroelectrically ordered state we need large δ. We may write this as $\delta = (R^2/a_0 D) \times (m^*/m)$, where a_0 is the Bohr radius and m^* is the effective mass of the electron. If $\tilde{R}$ and $\tilde{D}$ are R and D measured in nanometers, and $\tilde{m} \equiv (m^*/m)$, then $\delta \approx 18.9(\tilde{R}^2/\tilde{D})\tilde{m}$. We require that the rings do not intersect, so that $\tilde{D} \geq 2\tilde{R}$. Thus, the ability to achieve large values of δ in semiconductors will depend upon the value of the effective mass. If we set $\tilde{D} = 2\tilde{R}$, then for GaAs ($\tilde{m} = 0.06$) 1D arrays of rings with a radius greater than ~ 10 nm will be polarized. For AlAs ($\tilde{m} = 0.4$) the crossover radius is about 70 nm. Rings with a smaller radius will not spontaneously polarize, but instead be isotropic

It is well known that in 1D there is no ordered state for $T > 0$ for the Ising model. However, for small arrays over finite time intervals the system can order. To observe this behavior we want the characteristic energies of the system to be greater than the temperature. For the Coulomb energy $kT < e^2/D$, which we may write as $\tilde{D}T < 1.8 \times 10^3$ where T is in Kelvin. For the kinetic energy this means $kT < \hbar/2m^*R^2$; if we measure $(m/m^*)\tilde{R}^2 T > 40$ in the same units. For GaAs we can choose R to be about 14 nm at 4 K; choosing materials with a smaller effective mass or going to lower temperature allows us to increase the radius.

An AFE polarized ring array will scatter light at a wavelength commensurate with the inter-ring separation, D. In 1D there is a gap $\sqrt{2}\omega_0$, which we may write as $2\sqrt{2\tilde{m}}(a_0/D)^{3/2}$. For GaAs rings with a separation $D = 1000$ nm this gives $\omega \sim 6.0 \times 10^{10}$ Hz. The 2D arrays have a similar sized gap at zone center, but the gap vanishes at one zone edge. The excitation spectrum can be probed optically, but scattering at the edge of the zone is difficult due to the constraints imposed by conservation of energy and momentum. Typically, in such cases Raman scattering can be used to investigate the excitations.

While we have not explicitly addressed the 2D case here, much can be gleaned from our results. The 2D classical problem obviously has a finite temperature phase transition, as shown by our Monte Carlo simulations. The 2D quantum problem can be mapped onto the 3D XY model, which is known to order. We have performed simulations on the 2D case and find that it orders in a striped phase.

Finally, these calculations assume that each ring is singly occupied. This might be obtained by fabricating the rings upon a thin insulating layer covering a gate. By tuning the gate voltage we can bias the system so that it is energetically favorable for an electron to tunnel to the rings. The gate will also serve to cut off long-distance interactions between the rings, supporting the assumption of the nearest-neighbor interactions used here. Moreover, this paper serves to start investigation into a broad class of problems, such as rings occupied by an optically excited exciton/hole pair or perhaps by a small, varying number of electrons created by a random distribution of dopants.

The topic of quantum dot arrays and their correlations has obvious and useful analogies with solid-state models of crystalline arrays of atoms. In this paper we wish to point out that experimentalists have at their disposal a host of "unnatural atoms" analogs: rings, quantum dot quantum wells, quantum rice, etc. The electrons in these nanoscale constituents are confined to orbitals that may not have atomic analogs. Moreover, it may be possible to tune the shape of the constituent to optimize some desired collective property such as frustration in electric or magnetic polarization, high susceptibility or sensitivity to optical polarization of light. Even more rich behavior will develop if we allow electrons to tunnel between these nanoscale periodic structures.

Finally, the model we have introduced in this paper may have applications in implementation of quantum dot cellular automata (QDCA),[20] hence electronic devices for classical computation[21] or even quantum computation,[22] as well. In QDCA, quantum nanoscale devices such as quantum dots are used as "cells" and by manipulating the interactions inside and outside of the cells (between neighboring cells on an array) desired states can be achieved. In the original picture of QDCA, two electrons are trapped inside a cell (consisting of four dots) and by Coulomb interaction can take either of the two possible polarizations. Interaction between cells is also induced by Coulomb interaction or by application of global fields. In principle, any binary state for each cell can be considered as a representation for a "bit."

In our model, ground and excited states may play such a role. By tuning external control fields and interplay of Coulomb interactions, global state of the array can be altered.

Another potential application of linear arrays of atoms or spins may be in quantum state/information transfer. That is, the linear structure of the arrays together with tuned interactions may act as quantum information bus.[23] Due to existence of quantum coherence in the structure proposed here, we think that our model may show features useful for quantum computation or information processing. Detailed analysis of such applications is an interesting subject *per se*, but beyond the scope of this paper.

ACKNOWLEDGMENTS

The authors wish to thank Steve Girvin, Herbert Fertig, and Matthew Johnson for several useful discussions. This work was supported by NSF MRSEC Grant No. DMR-0080054 (B.R.) and NSF Grant No. EPS-9720651 (K.M.).

APPENDIX: TRANSVERSE FIELD ISING MODEL

In this section we explain how one can write the projection of Hamiltonian (19) into ground and first excited state subspace of $\hat{H}_0$ as a 1D transverse field Ising model [Eq. (20)]. In order to make the analysis easier we change the variables θ_i to staggered one, $(-1)^i\theta_i$. Defining $|0\rangle$ and $|1\rangle$ as ground and first excited states of $\hat{H}_0$ and E_0 and E_1 the corresponding eigenenergies we can write the up and down states (Fig. 15) as

$$|\uparrow\rangle = \frac{1}{\sqrt{2}}(|0\rangle + |1\rangle),$$

$$|\downarrow\rangle = \frac{1}{\sqrt{2}}(|1\rangle - |0\rangle). \tag{A1}$$

Now we define the creation and annihilation operators:

$$c_\uparrow^\dagger|\uparrow\rangle = c_\downarrow^\dagger|\downarrow\rangle = 0,$$

$$c_\uparrow^\dagger|\downarrow\rangle = |\uparrow\rangle, \quad c_\downarrow^\dagger|\uparrow\rangle = |\downarrow\rangle, \tag{A2}$$

and one can show that

$$[c_\alpha, c_\beta^\dagger] = \delta_{\alpha\beta}. \tag{A3}$$

Thus we can write Hamiltonian (19) as

$$\hat{H} = \sum_{i=1}^{N} \sum_{\alpha,\beta=\uparrow,\downarrow} \epsilon_{\alpha\beta} c_{i\alpha}^\dagger c_{i\beta} + \sum_{\langle ij\rangle} \sum_{klmn=\uparrow,\downarrow} V_{klmn}^{ij} c_{ik}^\dagger c_{jm}^\dagger c_{jn} c_{li}, \tag{A4}$$

in which i, j are spatial indices and

$$\epsilon = \frac{1}{2}\begin{pmatrix} \epsilon_0 & \Delta \\ \Delta & \epsilon_0 \end{pmatrix}, \tag{A5}$$

where $\epsilon_0 = E_1 + E_0$ and $\Delta = E_1 - E_0$. To calculate matrix elements of the potential we use a simple numerical Schrodinger equation solver to find the following quantities:

$$\langle\uparrow|\cos\theta|\uparrow\rangle = \langle\downarrow|\cos\theta|\downarrow\rangle \approx 0,$$

$$\langle\uparrow|\cos\theta|\downarrow\rangle = \langle\downarrow|\cos\theta|\uparrow\rangle \approx 0,$$

$$\langle\uparrow|\sin\theta|\uparrow\rangle \approx +1,$$

$$\langle\downarrow|\sin\theta|\downarrow\rangle \approx \langle\uparrow|\sin\theta|\downarrow\rangle = \langle\downarrow|\sin\theta|\uparrow\rangle \approx 0. \tag{A6}$$

In the above diagonal matrix elements of $\cos\theta$ are approximately zero because most of the wave function is localized around $\theta = \pm\pi/2$. For the same reason the diagonal matrix elements of $\sin\theta$ are ± 1. Using the above we can derive the potential in the following second quantized form:

$$\hat{V} = -2\delta\epsilon^2 \sum_{\langle ij\rangle} (c_{i\uparrow}^\dagger c_{j\uparrow}^\dagger c_{j\uparrow} c_{i\uparrow} - c_{i\uparrow}^\dagger c_{j\downarrow}^\dagger c_{j\downarrow} c_{i\uparrow} - c_{i\downarrow}^\dagger c_{j\uparrow}^\dagger c_{j\uparrow} c_{i\downarrow} + c_{i\downarrow}^\dagger c_{j\downarrow}^\dagger c_{j\downarrow} c_{i\downarrow}). \tag{A7}$$

Now we can use the Holstein-Primakov transformation[18] to construct the following SU(2) covariant operators for each lattice point:

$$S^+ = c_\uparrow^\dagger c_\downarrow, \quad S^- = c_\downarrow^\dagger c_\uparrow, \quad S^z = \frac{1}{2}(c_\uparrow^\dagger c_\uparrow - c_\downarrow^\dagger c_\downarrow). \tag{A8}$$

Using the above definitions and the fact that $c_\uparrow^\dagger c_\uparrow + c_\downarrow^\dagger c_\downarrow = 1$ for each lattice point we arrive at the following expression for Hamiltonian (19):

$$\hat{H} = -8\delta\epsilon^2 \sum_{i=1}^{N} S_i^z S_{i+1}^z + \Delta \sum_{i=1}^{N} S_i^x, \tag{A9}$$

in which $S^{x,y} = (S^+ \pm iS^-)/2$.

[1] Paul Harrison, *Quantum Wells, Wires and Dots: Theoretical and Computational Physics of Semiconductor Nanostructures* (Wiley, New York, 2005).
[2] M. Büttiker, Y. Imry, and R. Landauer, Phys. Lett. **96**, 365 (1983).
[3] R. Landauer and M. Buttiker, Phys. Rev. Lett. **54**, 2049 (1985).
[4] L. P. Levy, G. Dolan, J. Dunsmuir, and H. Bouchiat, Phys. Rev. Lett. **64**, 2074 (1990); V. Chandrasekhar, R. A. Webb, M. J. Brady, M. B. Ketchen, W. J. Gallagher, and A. Kleinsasser, *ibid.* **67**, 3578 (1991).
[5] S. Tarucha, D. G. Austing, T. Honda, R. J. vanderHage, and L. P. Kouwenhoven, Phys. Rev. Lett. **77**, 3613 (1996).
[6] K. Mullen, D. Loss, and H. T. C. Stoof, Phys. Rev. B **47**, 2689 (1993).
[7] K. L. Hobbs, P. R. Larson, G. D. Lian, J. C. Keay, and M. B. Johnson, Nano Lett. **4**, 167 (2004).
[8] A. Lorke, R. J. Luyken, A. O. Govorov, J. P. Kotthaus, J. M. Garcia, and P. M. Petroff, Phys. Rev. Lett. **84**, 2223 (2000).
[9] J. H. Lee, Z. M. Wang, Z. Y. Abuwaar, N. W. Strom, and G. J. Salamo, Nanotechnology **17**, 3972 (2006).

[10] Z. Y. AbuWaar, Yuriy I. Mazur, Jihoon H. Lee, Zhiming M. Wang, and G. J. Salamo, J. Appl. Phys. **101**, 024311 (2007).
[11] The Coulomb interaction scales inversely with distance, whereas the tunneling is exponentially suppressed. Indeed it would be experimentally difficult to achieve the limit where electrons can tunnel between rings. In the limit where electrons can tunnel from ring to ring the dynamics are much richer.
[12] A. Fetter and J. D. Walecka, *Quantum Theory of Many-Particle Systems* (McGraw-Hill, New York, 1971).
[13] Subdir Sachdev, *Quantum Phase Transitions* (Cambridge University Press, New York, 1999).
[14] Mats Wallin and S. M. Girvin, Phys. Rev. B **47**, 14642 (1993).
[15] J. Villain, J. Phys. (Paris) **36**, 581 (1975).
[16] J. V. Jose, L. P. Kadanoff, S. Kirkpatrick, and D. R. Nelson, Phys. Rev. B **16**, 1217 (1977).
[17] Mats Wallin, Erik S. Sorensen, S. M. Girvin, and A. P. Young, Phys. Rev. B **49**, 12115 (1994).
[18] Assa Auerbach, *Interacting Electrons and Quantum Magnetism* (Springer-Verlag, New York, 1994).
[19] M. Bayer, M. Korkusinski, P. Hawrylak, T. Gutbrod, M. Michel, and A. Forchel, Phys. Rev. Lett. **90**, 186801 (2003).
[20] G. S. Lent, P. D. Tougaw, W. Porod, and G. H. Bernstein, Nanotechnology **4**, 49 (1993); see also http://www.nd.edu/qcahome/
[21] P. D. Tougaw and C. S. Lent, J. Appl. Phys. **75**, 1818 (1994).
[22] G. Toth and C. S. Lent, Phys. Rev. A **63**, 052315 (2001).
[23] M. Christandl, N. Datta, A. Ekert, and A. J. Landahl, Phys. Rev. Lett. **92**, 187902 (2004).